ISBN: 978-3-95450-232-5 ISSN: 2673-7000 doi:10.18429/JACoW-NAPAC2022-TUPA77

X-BAND CAVITY BASED LONGITUDINAL PHASE SPACE LINEARIZATION AT THE UCLA PEGASUS PHOTOINJECTOR

P. Denham *, A. Ody, P. Musumeci
Department of Physics and Astronomy,
University of California at Los Angeles, Los Angeles, CA 90095, USA

Abstract

Due to the finite bunch length, photoemitted electron beams sample RF-nonlinearities that lead to energy-time correlations along the bunch temporal profile. This is an important effect for all applications where the projected energy spread is important. In particular, for time-resolved single shot electron microscopy, it is critical to keep the beam energy spread below 1×10^{-4} to avoid chromatic aberrations in the lenses. Higher harmonic RF cavities can be used to compensate for the RF-induced longitudinal phase space nonlinearities. Start-to-end simulations suggest that this type of compensation can reduce energy spread to the 10^{-5} level. This work is an experimental study of x-band harmonic linearization of a beam longitudinal phase space at the PEGASUS facility, including developing high-resolution spectrometer diagnostics to verify the scheme.

INTRODUCTION

Controlling the details of the longitudinal phase space in high brightness beams is of paramount importance. Energy correlations along the bunch temporal coordinate affect the emittance compensation process, how lenses act on the transverse beam size and generally any application where monochromatic beams are required.

If a short (< 1 ps) electron bunch is generated at the injector (either by using a short laser pulse or by some form of beam compression), in an S-band RF acceleration cavity (2.856 GHz), the beam occupies less than 1 degree of RF phase and the variation of the beam energy along the beam can be neglected (especially when compared to the one induced by space charge effects). Conversely, if long beams are needed the spread in particle energies induced by the RF curvature can be significant and have a dominant effect on the beam evolution.

One scheme that has been put forward to compensate the RF-induced energy spread is the use of higher harmonic RF cavity to impart equal and opposite energy correlation and linearize the longitudinal phase space distribution [1, 2]. In this paper, we present our current status of experiments running at the UCLA Pegasus laboratory aiming to generate ultralow (< 1e-4) energy spread beams by compensating the higher order correlations in longitudinal phase space with an X-band RF cavity. In order to improve the energy resolution of the spectrometer currently installed on the beamline we added to the setup a pinhole to reduce the transverse emittance and a quadrupole to magnify the dispersion.

* pdenham@physics.ucla.edu

The data indicate that we can compensate up to 2nd order, the beam energy spread in agreement with start-to-end simulations of the injector column. These measurements suggest that chromatic aberrations in a single shot time-resolved TEM experiment, using the PEGASUS injector can be reduced to a small level similar to space charge aberrations, validating the feasibility of using the PEGASUS injector for single shot TEM with 10 nm-10 ps spatio-temporal resolution [3–5].

PEGASUS BEAMLINE AND X-BAND CAVITY DESCRIPTION

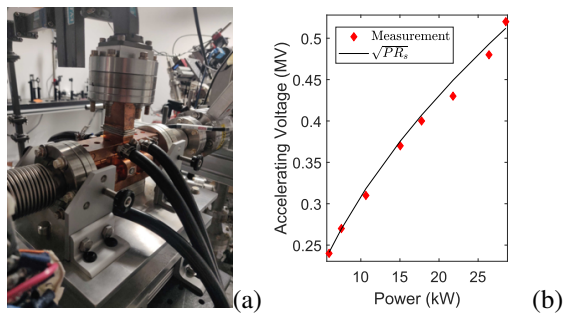

(a) (b)

Figure 1: (a) X-band cavity installation at PEGASUS. (b) Shunt Impedance measurements of X-band cavity.

The injector layout is shown in Fig. 1. The photocathode is illuminated by a 266 nm drive Ti:Sa laser. The temporal profile of the laser is stretched from the initial 40 fs RMS temporal duration to a nearly uniform flat-top > 10 ps long pulse. To this end, we use 3 α-BBO crystals with respective lengths 8.75mm, 4.375mm, 2.1875mm, which splits the single 40fs beam into 8 beamlets spanning 13.3 ps [6]. The pulses are then sent through a MgF_2 crystal and a prism to further stretch each pulse and facilitate temporal overlap. After that, the laser is focused onto a NaKSb photocathode by a 175 mm focal length lens through a 72 degrees oblique incidence vacuum port. The oblique port allows the final lens to be brought closer to the cathode surface [7], but the illumination of the cathode is asymmetric. The alkali-antimonide photocathode is inserted in a BNL/SLAC/UCLA 1.6 cell clamped S-band RF gun [8] using a specially designed load-lock chamber. Note that operation of these cathodes using UV laser results in a relatively large MTE of 2 eV, which is not important for this particular experiment. A focusing solenoid immediately after the gun is followed by a 9.6 GHz x-band linearizing cavity and S-band Linac [9] centered 1.1 m and 1.7 m downstream of the cathode respectively.

ISBN: 978-3-95450-232-5 ISSN: 2673-7000 doi:10.18429/JACoW-NAPAC2022-TUPA77

The X-band cavity and S-band Linac are 0.1 m and 0.62 m in length respectively. The installation of the X-band cavity is shown in Fig. 1. Between the X-band and the booster linac is an integrated current transformer for non destructive measurements of the bunch charge. A dipole positioned at the exit of the linac that is used to measures beam energy and energy spread, which we initially used to characterize the cavity shunt impedance, phase and amplitude stability.

A cavity frequency of 9.6GHz simplifies the synchronization with the S-band gun and linac system. A part of the low level 2.856 GHz seed used to drive the S-band klystron is frequency divided by 36 to 79.33 MHz, then split in two. A fraction of the power goes to the synchrolock system to synchronize the laser to the RF system. The other portion is frequency multiplied by 121, pre-amplified to 1 W level, and then further amplified to up to 40 kW with a small X-band klystron, to simultaneously phase lock the X-band system to the laser at the operating frequency of 9.599 GHz.

The shunt impedance of the X-band cavity was measured using the dipole just after the linac. Specifically, the accelerating voltage was determined from the energy gain of the beam at the maximum accelerating phase as the input power was varied. The results are shown in Fig. 1). The power fit to the data indicates a shunt impedance of 8.69 MΩ in good agreement with the cavity design. Given the klystron power budget, the maximum field achievable in the cavity is 10 MV/m.

We also assessed the amplitude and phase stability of the RF system. Amplitude stability was quantified by setting the X-band to the maximum accelerating phase. where the beam energy is linearly dependent on the cavity amplitude and essentially insensitive to the phase. Over a hundred shots, the rms amplitude fluctuations were 2×10^{-3}. Alternatively, phase fluctuations were quantified at the zero crossing, where the beam energy changes linearly with phase offset. Again, the energy deviations were collected over a 100 shots. After removing long term drift, we found rms phase fluctuations to be 1°. With respect to the intended applications of the X-band cavity, the phase fluctuations will have a bigger impact than the amplitude fluctuations on stable compensation.

ANALYTICAL COMPENSATION AND BEAM DYNAMICS SIMULATION

Here we analyze analytically and numerically third-order energy spread compensation. At the exit of the gun, the LPS has a dominating correlation between energy and position (relative to the beam centroid) of the form $\gamma(z) = \gamma_0 \cos(kz + \phi_0)$ where γ_0 is a normalized cavity voltage, k is the cavities spatial wave-number, and ϕ_0 is the operational phase of the gun. In the following we will assume that the longitudinal positions of the particles are frozen during propagation. In practice depending on their energy the particles can move towards the tail or head of the beam. Mathematically, for a drift distance characterized by L, this is a good approximation if $\sin(\phi_0)kL/\gamma^2 << 1$. In this case, we can reasonably estimate the LPS RF correlations after the sequence of gun, X-band, and linac to be $\gamma(z) = \gamma_0 \cos(kz+\phi_0)+\alpha_x \cos(k_x z+\phi_x)+\alpha_L \cos(kz+\phi_L)$. where $\alpha_{x,L}$ are the normalized voltages of the X-band cavity and linac respectively. The correlation can be Taylor expanded to 3rd order, $\gamma(z) = c_0 + c_1 z + c_2 z^2 + c_3 z^3 + O(z^4)$. Typically, the optimum gun phase and voltage are determined by other considerations (emittance, charge, etc.). and the linac voltage can be changed to tune the final beam energy. The expansion coefficients, c_1, c_2, and c_3 are the main contribution to energy spread. They all vanish if the configuration has the x-band phase set to π, the linac phase such that $\sin(\phi_L) = -\gamma_0 \sin(\phi_0)/\alpha_L$, and finally the X-band voltage, $\alpha_x = \left(\gamma_0 \cos(\phi_0) + \sqrt{\alpha_L^2 - \gamma_0^2 \sin^2(\phi_0)}\right) k^2/k_x^2$, then c_0 is given by:

$$c_0 = \left(\gamma_0 \cos(\phi_0) + \sqrt{\alpha_L^2 - \gamma_0^2 \sin^2(\phi_0)}\right)\left(1 - \frac{k^2}{k_x^2}\right) \quad (1)$$

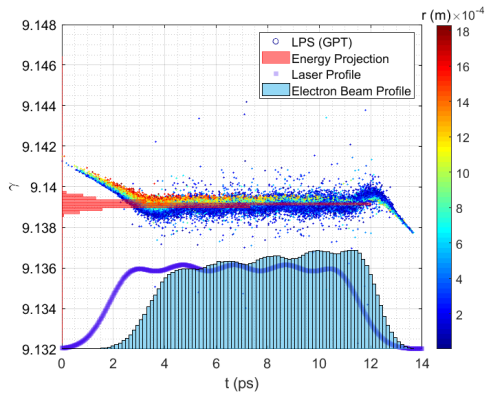

Figure 2: Longitudinal phase space 3 m downstream of the gun, after the linearizer and linac cavities, where the beam coasts with 2×10^{-5} relative energy spread. The LPS is color coded with particle radius from core. Energy and temporal projections are shown along the corresponding axes. The input laser profile (initial temporal distribution) is also shown.

Table 1: Simulation Beam Parameters

Parameter	Value
Beam Kinetic Energy	4.2 MeV
Relative Energy Spread	2×10^{-5}
Normalized Emittance	130 nm· rad

An injector simulation was performed using the General Particle Tracer (GPT) software, including smooth 3D space charge effects and comparing the results to the effect of Coulomb scattering modeled using the spacecharge3Dtree option [10]. The simulated beam is initialized with an MTE of 2 eV, 250 fC bunch charge, 50 μm rms transverse size, and 10 ps (FWHM) duration. The analytical estimates just presented provide an excellent starting point for the optimization. In Table 1 we list the results of the simulation at a

ISBN: 978-3-95450-232-5 ISSN: 2673-7000 doi:10.18429/JACoW-NAPAC2022-TUPA77

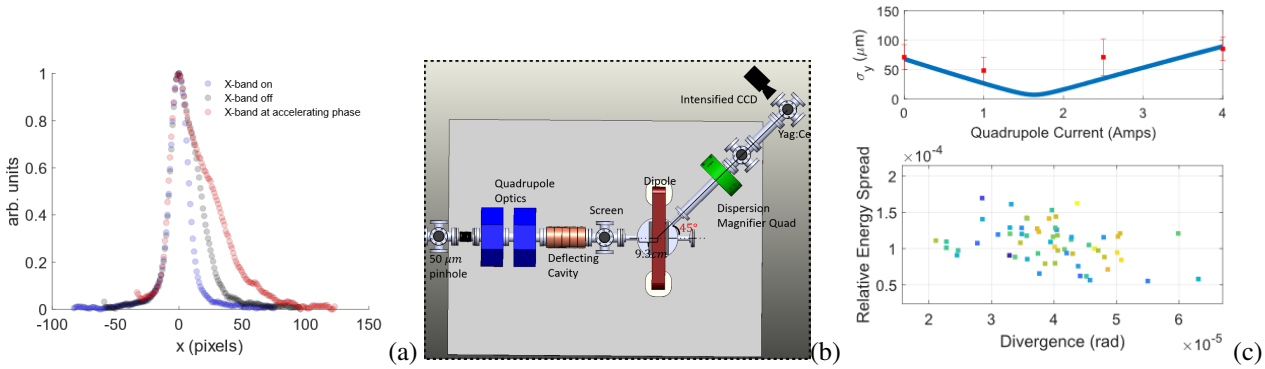

Figure 3: (a) Shows a comparison of horizontal projections taken at spectrometer 1, with x-band on, off, and at accelerating phase. (b) Shows a top down cartoon view of the high resolution spectrometer layout. (c) Vertical quadrupole scan reconstruction and energy spread measurements at spectrometer 2.

screen 3 m downstream of the cathode. The beam's LPS at this location is shown in Fig. 2. Notably, all RF correlations other than $0th$ order have been removed from the LPS. The remaining spread in energy is mainly due to smooth space charge effects. In order to minimize these, the initial temporal profile should be free of temporal modulations, and the rise and fall times of the laser pulse should be sharp. Transverse uniformity of the electron beam is difficult to maintain because the beams inherit at emission a Gaussian angular spread from the photocathode. The outlying particles in the LPS are due to Coulomb collisions, which overall are found to contribute negligibly to the overall measure of energy spread at the level of beam current densities present in the injector.

HIGH RESOLUTION SPECTROMETER MEASUREMENTS

The energy spectra after compensation recorded on the first spectrometer are shown in Fig. 3(a). The profiles indicated suppression of second-order RF curvature which manifests manifests as an asymmetry in the energy projections. Unfortunately, we could not accurately distinguish the relative energy spread because of the large betatron contribution to the horizontal beam size which limits the energy resolution in this setup, so we developed a spectrometer with a higher resolution.

In our second spectrometer line located nearly 4 m downstream of the Pegasus linac, we placed a pinhole with radius $r = 50$ µm , 0.5 m upstream of a round-pole dipole magnet. The pinhole reduces the spot size and subsequently the emittance by nearly two orders of magnitude. With a good approximation we can assume a waist condition at the pinhole as the beam is very gently focused with the gun solenoid there. Additionally, a quadrupole at the mid point of a 0.5 m dispersion arm is used to increase dispersion and reconstruct the vertical trace space. The entire layout of the high-resolution spectrometer is shown in Fig. 3(b).

The x-band system stability made it challenging to consistently transmit the beam through the pinhole, so we chose to benchmark the resolution of the second spectrometer with a beam generated without the use of the x-band linearizer. We found a working point where the beam is compressed by a factor of 4 so that only a small interval of RF phase is sampled in the linac and the energy spread can be maintained below 1e-4.

After sending the beam through the spectrometer, we saw a scattered background on top of a transmitted beam (due to the pinhole only being 30um thick). which can be filtered out thresholding the image intensity at the 2 sigma value of the entire beam. Then a vertical quadrupole scan reconstruction yielded a spot size in agreement with the pinhole size, a nearly zero α twiss parameter, and divergence of 4×10^{-5}. The quadrupole scan fit is shown in the top panel of Fig. 3 (c).

Assuming a round beam (every active element in the beamline is cylindrically symmetric) we can use this information to retrieve the energy spread by algebraically subtracting the betatron contributions from the final horizontal spotsize. The explicit formula for the relative energy spread is:

$$\sigma_\delta = \frac{1}{R_{16}} \sqrt{\langle x^2 \rangle - \langle y^2 \rangle \frac{R_{12}^2}{R_{34}^2} - \left(R_{11}^2 - \frac{R_{12}^2 R_{33}^2}{R_{34}^2} \right) r^2/4} \quad (2)$$

Eq. 2 is valid if the trace space is at a waist after the pinhole. Mathematically, the waist condition is met if $\sigma_{x0} >> r\alpha$, where σ_{x0} and α are the spot size and twiss parameter before the pinhole. With Eq. 2 we measured the energy spread and divergence shot-to-shot; the results, color coded with intensity, are shown in the bottom panel of Fig. 3(c). Most shots consistently yielded divergence of $4 \times 10^{-5} \pm 5 \times 10^{-6}$ rad, in accordance with the vertical scan, and relative energy spread of $1 \times 10^{-4} \pm 3 \times 10^{-5}$, with many shots under 1×10^{-4}.

ACKNOWLEDGEMENTS

This work was partially supported by NSF grant PHY-1734215 and DOE grant No. DE-SC0009914

ISBN: 978-3-95450-232-5 ISSN: 2673-7000 doi:10.18429/JACoW-NAPAC2022-TUPA77

REFERENCES

[1] B. Zeitler, K. Floettmann, and F. Gruner, "Linearization of the longitudinal phase space without higher harmonic field", *Phys. Rev. ST Accel. Beams*, vol. 18, p. 120102, Dec. 2015. doi:10.1103/physrevstab.18.120102

[2] K. Floettmann, "Generation of sub-fs electron beams at few-MeV energies", *Nucl. Instrum. Methods Phys. Res., Sect. A*, vol. 740, pp. 34-38, 2014. doi:10.1016/j.nima.2013.12.031

[3] R. Li and P. Musumeci, "Single-shot MeV transmission electron microscopy with picosecond temporal resolution", *Phys. Rev. Appl.*, vol. 2, no. 2, p. 024003, 2014. doi:10.1103/PhysRevApplied.2.024003

[4] P. Denham and P. Musumeci, "Space-Charge Aberrations in Single-Shot Time-Resolved Transmission Electron Microscopy", *Phys. Rev. Appl.*, vol. 15, p. 024050, 2021. doi:10.1103/PhysRevApplied.15.024050

[5] D. Cesar *et al.*, "Demonstration of Single-Shot Picosecond Time-Resolved MeV Electron Imaging Using a Compact Permanent Magnet Quadrupole Based Lens", *Phys. Rev. Lett.*, vol. 117, p. 024801, 2016. doi:10.1103/PhysRevLett.117.024801

[6] P. Musumeci, R. Li, and A. Marinelli, "Nonlinear Longitudinal Space Charge Oscillations in Relativistic Electron Beams", *Phys. Rev. Lett.*, vol. 106, p. 184801, 2011. doi:10.1103/PhysRevLett.106.184801

[7] J. Maxson, D. Cesar, G. Calmasini, A. Ody, P. Musumeci, and D. Alesini, "Direct measurement of sub-10 fs relativistic electron beams with ultralow emittance", *Phys. Rev. Lett.*, vol. 118, p. 154802, 2017. doi:10.1103/PhysRevLett.118.154802

[8] D. Alesini *et al.*, "New technology based on clamping for high gradient radio frequency photogun" *Phys. Rev. ST Accel. Beams*, vol. 18, p. 092001, 2018. doi:10.1103/PhysRevSTAB.18.092001

[9] N. Barov, X. Chang, R. H. Miller, and D. J. Newsham, "Development of the Dual Slot Resonance Linac", in *Proc. IPAC'12*, New Orleans, LA, USA, May 2012, paper TH-PPC044, pp. 3383–3385.

[10] G. Poplau, U. van Rienen, B. van der Geer and M. de Loos, "Multigrid algorithms for the fast calculation of space-charge effects in accelerator design", *IEEE Transactions on Magnetics*, vol. 40, no. 2, pp. 714-717, 2004. doi:10.1109/TMAG.2004.825415